

# Direct observation of lateral current spreading in ridge waveguide lasers using scanning voltage microscopy

D. Ban<sup>a)</sup> and E. H. Sargent

*Department of Electrical and Computer Engineering, University of Toronto, 10 King's College Road, Toronto, Ontario, M5S 3G4, Canada*

K. Hinzer,<sup>b)</sup> St. J. Dixon-Warren, A. J. SpringThorpe,<sup>a)</sup> and J. K. White

*Nortel Networks Optical Components, 3500 Carling Avenue, Ottawa, Ontario, K2H 8E9, Canada*

(Received 4 December 2003; accepted 7 April 2003)

We report results of two-dimensional (2D) local voltage measurement of the transverse cross section of operating multiquantum-well ridge-waveguide (RWG) lasers. We observe lateral nonuniformity of local voltage in the *n*-cladding layers of the laser and attribute the voltage variation to 2D carrier transport effect within the RWG lasers. The quantitative evaluation of this effect indicates the local vertical current density to be ~40% smaller at the edge of the ridge than at its center. Our results demonstrate the strength and application of scanning voltage microscopy technique in quantitatively delineating 2D current flow in operating optoelectronic devices. © 2003 American Institute of Physics. [DOI: 10.1063/1.1581982]

Ridge-waveguide (RWG) lasers are technologically important for their applications in optical communication systems.<sup>1–3</sup> Their performance is highly dependent on current flow to the active region.<sup>4–6</sup> Lateral current spreading in this region can significantly affect the device performance and can result in a reduced efficiency above threshold,<sup>7</sup> a considerable degradation of operation in the fundamental transverse mode operation (shape of the mode), a perturbation of the longitudinal mode via the lateral mode instability,<sup>8</sup> and a rise in intermodulation distortion under direct modulation.<sup>9,10</sup> There has been significant interest in quantifying the amount of lateral current spreading present in specific designs and the epitaxial layers from which the lateral current originates. This issue has been tackled using experimental observation of the external performance of the devices in conjunction with modeling of the internal operation of the laser. For example, Evans and co-workers<sup>4</sup> developed an analytical model to evaluate the impacts of lateral current spreading on the performance of multiquantum-well (MQW) InGaAsP/InP RWG lasers. They reported that the lateral current spreading in narrow ridge width lasers (less than 5 μm) is significant—up to 42% of the injected current escapes from the index-guided region at threshold for a 2 μm ridge width. As well, Belenky *et al.*,<sup>11</sup> by measuring the gain and loss and modeling the optical confinement in buried heterostructure lasers with varied mesa widths, concluded that up to 30% of the threshold current in single mode devices does not contribute to active region pumping.

Scanning voltage microscopy (SVM),<sup>12,13</sup> based on atomic force microscopy, is a direct method for measuring two-dimensional (2D) maps of the internal potential profile within actively driven semiconductor devices, and thus provides a direct and quantitative view into the internal behavior

of operating semiconductor devices. In this letter, we report the application of SVM to InAlGaAs/InP ridge-waveguide MQW lasers driven actively above the lasing threshold. We present 2D voltage profiles with high spatial resolution (sub 20 nm) of the transverse cross section of lasing devices. We complement these results using scanning spreading resistance microscopy (SSRM) measurements, which delineate the transverse cross section beneath the ridge and resolve individual quantum-well/barrier layers. We report measurement of the lateral voltage distribution within different vertical layers of the RWG laser. Our results provide a direct and quantitative picture of the impact of 2D carrier transport.

We carried out both SSRM and SVM using a commercial atomic force microscope (AFM) system (Nanoscope III, Dimension 3100, Digital Instruments with SSRM applications module). In SVM mode, a conductive AFM tip was used to measure the voltage profile on a surface. The probe was scanned in contact mode over the transverse cross section of the device. The contact force was set sufficiently high such that the tip mechanically penetrated the native oxide layer at the sample surface to establish a good electrical contact. The local voltage (with reference to *p* side of the device) was measured by a voltmeter having a high input impedance (Keithley 6517 A). The spatial resolution was on the same order as the radius of the AFM tip (~20 nm). Details of the experimental setup can be found in Ref. 14.

The RWG laser samples (ridge width = 2.4 μm) were metallized with ohmic contacts. A polish-free sample preparation procedure was conducted to produce clean bar cleaves devoid of fracture lines and to minimize overedge current leakage. The sample bar with 2 mm long Fabry–Perot cavities was then mounted with the cleaved edge facing up in a custom metal clamp. The current–voltage characteristics of the samples were measured before, during, and after the SVM experiment. No change was observed in the electrical behavior of the device. The topographic AFM image of the sample surface, obtained simultaneously with the SSRM and SVM data, showed no perceptible features.

<sup>a)</sup>Also at: Institute for Microstructural Sciences, National Research Council, Ottawa, Ontario, Canada K1A 0R6.

<sup>b)</sup>Author to whom correspondence should be addressed; electronic mail: khinzer@bookham.com

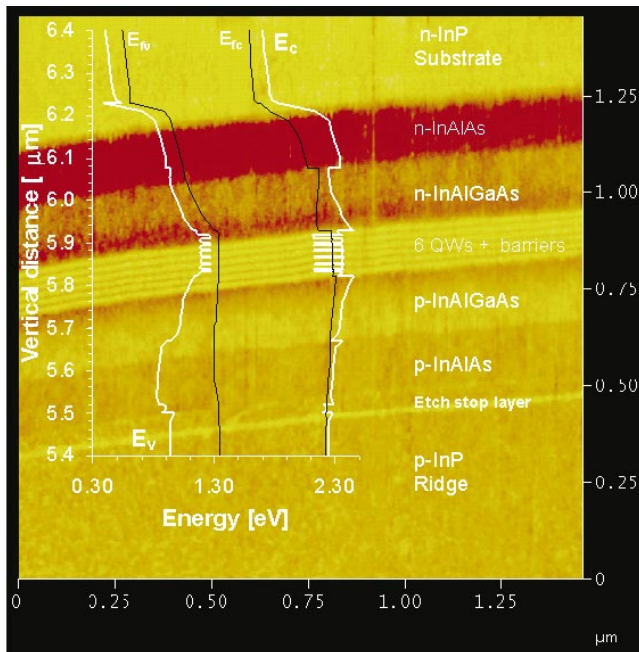


FIG. 1. (Color) SSRM image of RWG laser in transverse cross section. The tip bias was 1.0 V and the scan rate was 0.5 Hz. The inset shows the band diagram of the laser above threshold (valence band:  $E_v$ , conduction band:  $E_c$ , Fermi level for the valence band:  $E_{fv}$ , and Fermi level for the conduction band:  $E_{fc}$ ).

SSRM was first conducted to examine the cross section of the RWG MQW lasers under zero bias. Figure 1 shows a 2D SSRM image on a freshly cleaved facet of the laser sample. A small scan size was set in the measurement to obtain high spatial resolution so as to resolve individual quantum wells. The core laser structures are labeled in Fig. 1, including the MQW active region, and the *n*-cladding layers (*n*-InAlAs and *n*-InAlGaAs), the *p*-cladding layers (*p*-InAlAs and *p*-InAlGaAs), the *n*-InP atop the substrate all grown by molecular-beam epitaxy, and at the bottom, the *p*-InP layer for ridge definition grown by metalorganic chemical vapor deposition. The quantum wells of the device appear as six bright lines in the middle of the image, illustrating the high spatial resolution (sub 20 nm) of this technique. The difference in doping types (*n* or *p* doped), doping concentration, and material composition of each semiconductor layer gives rise to substantial color contrast in the SSRM image, leading to clear resolution of the nanometric features beneath the ridge. The inset of Fig. 1 shows the flat-band energy diagram of the laser operating under forward bias. The calculation was done using a commercial 2D laser simulation tool.<sup>9</sup> Note that the *n*-InAlAs is an energetic barrier for electrons due to its type-II band offset with InP and InAlGaAs.

Figure 2 shows the 2D SVM image in transverse cross section of a RWG MQW laser biased under a forward current injection of 100 mA. The device is operating 40 mA above threshold and is emitting more than 10 mW in output power. The ridge structure and some buried layers beneath the top surface, such as the etch stop layer, the MQW active region, the *n*- and *p*-cladding layers and the *n* substrate, are resolved in the SVM image and correlate with the structure shown in Fig. 1. For the 2D SVM map to display the measurement as clearly as possible, the voltage scale is inverted and goes

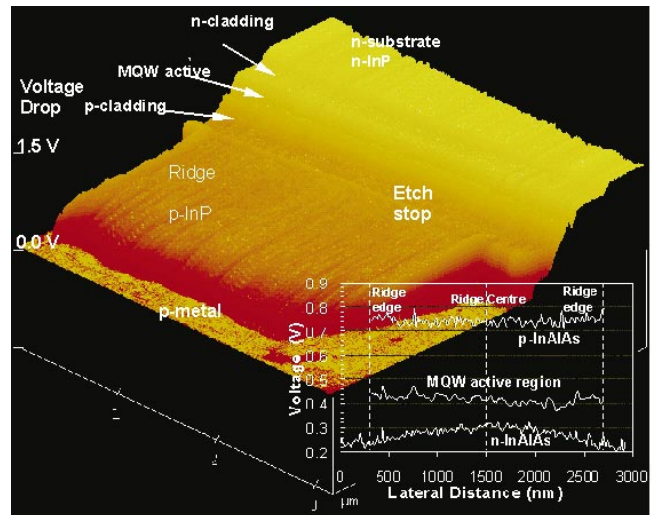


FIG. 2. (Color) 2D local voltage drop image of the RWG laser in transverse cross section (Note: to display the measurement as clearly as possible, the voltage scale is inverted). The laser was biased 40 mA above lasing threshold (a forward bias of 1.372 V). The inset shows the full lateral cross-sectional voltage profiles sampled in three vertical layers: *n* InAlAs, MQW active region, and *p* InAlAs. The *n* InAlAs layer displays a nonuniform lateral voltage distribution.

from 0 V up to 1.5 V. The accumulated voltage drop from the *p* metal to the substrate measured from the SVM agrees with the externally applied voltage. Substantial voltage drops can be observed at some interfaces of two adjoining layers, including the *p*-metal-to-*p*-InP interface and the interfaces between the MQW active region and adjacent *p* and *n* injectors.

It can be seen in the SVM image that the lateral (parallel to the ridge top surface) voltage profile within the *n*-cladding layer is not uniform from one edge to the other across the ridge. This lateral nonuniformity in voltage is more readily observed in the cross-sectional analysis as shown in the inset. The voltage within the *p*-InAlAs layer and MQW active region is flat to within the experimental error; however, a difference of up to  $\sim$ 75 mV can be measured within the *n*-InAlAs layer. The curvature of the *n*-InAlAs trace is almost symmetric with respect to the ridge center as would be expected due to the symmetry of the device.

The nonuniform lateral voltage distribution within RWG lasers, as revealed in Fig. 2, is directly related to lateral current profiles. It therefore merits in-depth investigation and further discussion. Figure 3 shows the laterally cross-sectional voltage profiles as the RWG laser was biased at an elevated current injection, i.e., 150 mA, where the device is emitting more than 15 mW of power. As expected, increased current injection gives rise to more severe lateral current spreading and consequently increases the nonuniformity in the lateral voltage distribution. This is observed in the lateral voltage difference as measured in the *n*-InAlAs layer, which is around 200 mV at 150 mA (Fig. 3), while only 75 mV at 100 mA (Fig. 2).

Figure 3 provides a depth profile analysis of the laterally cross-sectional voltage distribution. It shows a different curvature of the voltage profiles, across half of the laser ridge, within the layers at different depths underneath the top surface of the RWG laser. For layers within or close to the ridge definition, such as the *p*-InP, *p*-InAlAs, and the MQW ac-

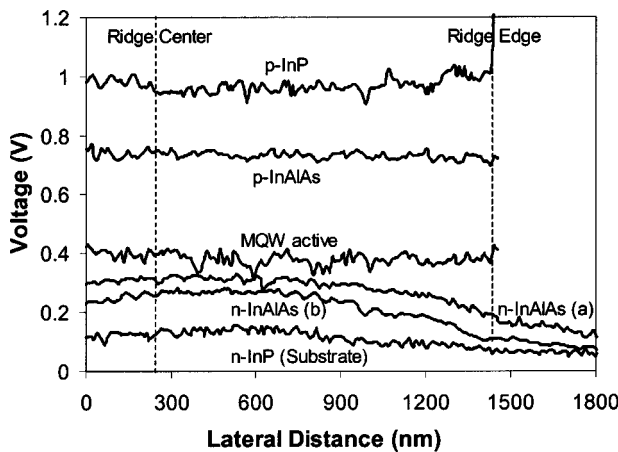


FIG. 3. Lateral cross-sectional local voltage profiles, across half the laser ridge, of the layers at different depth from the *n* InP substrate (bottom trace) to the *p* InP near the top of the ridge (top trace). The laser was forward biased at 150 mA. *n*-doped layers show nonuniform lateral voltage distribution. The curves of *n* InAlAs (a) and (b) are taken  $\sim$ 60 nm apart with trace (a) sampled at depth closer to the MQW and trace (b) sampled closer to the *n* InP layer.

tive region, the lateral voltage profile is almost uniform from the center to the edge of the ridge within experimental error. However, the lateral voltage is nonuniform in the layers below the ridge definition (i.e., *n* InAlAs) and the region inside the *n* substrate. The two curves, as labeled by *n* InAlAs [Fig. 3(a)] and [Fig. 3(b)] and sampled  $\sim$ 100 nm and  $\sim$ 40 nm from the *n*-InAlAs–InP interface, respectively, both exhibit a significant curvature but have a slight disparity in lateral voltage variation. The voltage differs along the lateral direction up to  $\sim$ 200 mV in the curve *n*-InAlAs [Fig. 3(a)] and a reduced value of  $\sim$ 170 mV in *n* InAlAs [Fig. 3(b)]. The bottom curve is sampled within the *n* substrate close to the *n*-InAlAs layer (less than 100 nm away from the interface), which shows a less than 100 mV difference in voltage in lateral direction.

Since ridge definition was achieved by etching the semiconductor layers on the *p*-doped side up to the etch stop layer located close to the active layer, current confinement in *p*-doped layers and even in the MQW active region is well established by the ridge boundary. The lateral voltage profile is consequently uniform across the ridge region. The absence of the ridge boundary results in 2D carrier transport observed in the layers on the *n*-doped side, which is expected to be the most significant in the layer closest to the MQW active region. The strong lateral voltage nonuniformity in the *n*-InAlAs layer relates also to band alignment: As shown in the inset of Fig. 1, the conduction-band edge of the *n*-InAlAs layer is higher than the adjacent layers. Electrons experience an energetic barrier when flowing across the *n*-InAlAs layer and thus more voltage drop would be required for driving the drifting current. This explains the considerable curvature of the lateral voltage profile in *n*-InAlAs layer and the reduced lateral voltage nonuniformity in the *n* substrate.

The 2D carrier transport effect may be estimated quantitatively by examining the SVM data in more detail. Since the *n*-InAlAs [Fig. 3(a)] lateral voltage curve is sampled at a depth that is 400 nm away from the MQW region, we can

assume drift current dominates beyond that depth until the *n*-contact metal layer. The vertical component of local current density ( $j$ ) for this region is given by

$$j = -\sigma \nabla V, \quad (1)$$

where  $\sigma$  is the local conductivity and  $\nabla V$  is the voltage gradient along the direction perpendicular to the semiconductor junctions. For an essentially homogeneous conductivity, the voltage gradient drives the current density. The voltage drop from the *n*-InP to the *n*-InAlAs [Fig. 3(a)] layers is  $\Delta V_c = 190 \pm 15$  mV at the center, or  $\Delta V_e = 114 \pm 15$  mV at the edge of the ridge, as read from Fig. 3. The ratio of the local vertical current density at the edge and center is then estimated to be

$$\frac{j_e}{j_c} = \frac{\sigma \nabla V_e}{\sigma \nabla V_c} = \frac{\Delta V_e}{\Delta V_c} = \frac{114}{190} = 0.6. \quad (2)$$

The result indicates the local vertical current density at the edge is around 40% smaller than that at the center of the ridge.

In summary, we present the results of the first SVM measurement of operating MQW RWG lasers on the nanometer scale. The 2D carrier transport effect in the RWG lasers is investigated directly and quantitatively via experimental means. By examining the lateral nonuniformity of the local voltage, we find that the local current density at the edge is  $\sim$ 40% smaller than that at the center of the 2.4  $\mu$ m wide ridge under 150 mA forward bias. SVM provides quantitative 2D internal voltage distribution of the transverse cross section of actively driven devices with high spatial resolution and holds great potential application in the device design, fabrication, and optimization of RWG and other laser devices.

The authors would like to thank Scott Kuntze for the band diagram. Nortel Networks Optical Components was divested to Bookham Technology (November 2002).

- <sup>1</sup>H. Konig, J. P. Reithmaier, A. Forchel, J. L. Gentner, and L. Goldstein, *Appl. Phys. Lett.* **73**, 2703 (1998).
- <sup>2</sup>M. Aoki, M. Komori, T. Tsuchiya, H. Sato, K. Nakahara, and K. Uomi, *IEEE J. Sel. Top. Quantum Electron.* **3**, 672 (1997).
- <sup>3</sup>A. B. Massara, K. A. Williams, I. H. White, R. V. Penty, A. Galbraith, P. Crump, and P. Harper, *Electron. Lett.* **35**, 1646 (1999).
- <sup>4</sup>G. J. Letal, J. G. Simmons, J. D. Evans, and G. P. Li, *IEEE J. Quantum Electron.* **34**, 512 (1998).
- <sup>5</sup>S. Y. Hu, S. W. Corzine, K.-K. Law, D. B. Young, A. C. Gossard, L. A. Coldren, and J. L. Merz, *J. Appl. Phys.* **76**, 4479 (1994).
- <sup>6</sup>M. Legge, G. Bacher, S. Bader, A. Forchel, H.-J. Lugauer, A. Waag, and G. Landwehr, *IEEE Photonics Technol. Lett.* **12**, 236 (2000).
- <sup>7</sup>A. V. Harton and C. G. Fonstad, *J. Appl. Phys.* **72**, 2575 (1992).
- <sup>8</sup>M. Achtenhagen and A. Hardy, *Appl. Phys. Lett.* **74**, 1364 (1999).
- <sup>9</sup>J. Piprek, J. K. White, and A. J. SpringThorpe, *J. Quantum Electron.* **38**, 1253 (2002).
- <sup>10</sup>G. H. B. Thompson, *Physics of Semiconductor Laser Devices* (Chichester, Wiley, 1980).
- <sup>11</sup>G. Belenky, L. Shterengas, C. L. Reynolds, Jr., M. W. Focht, M. S. Hybertsen, and B. Witzigmann, *IEEE J. Quantum Electron.* **38**, 1276 (2002).
- <sup>12</sup>T. Trenkler, R. Stephenson, P. Jansen, and W. Vandervorst, and L. Hellermanns, *J. Vac. Sci. Technol. B* **18**, 586 (2000).
- <sup>13</sup>D. Ban, E. H. Sargent, St. J. Dixon-Warren, I. Calder, A. J. SpringThorpe, R. Dworschak, G. Este, and J. K. White, *Appl. Phys. Lett.* **81**, 5057 (2002).
- <sup>14</sup>D. Ban, E. H. Sargent, St. J. Dixon-Warren, I. Calder, T. Grevatt, G. Knight, and J. K. White, *J. Vac. Sci. Technol. B* **20**, 2401 (2002).